

# Permeation and Desalination of Salt Water through Nanomembrane

Pooja Sahu<sup>1,2</sup>, \*Sk. Musharaf Ali<sup>1,2</sup>

<sup>1</sup>Chemical Engineering Division, Bhabha Atomic Research Centre, Mumbai-400085, India

<sup>2</sup>Homi Bhabha National Institute, Mumbai-400094, India

### ABSTRACT

The nanoscopic assessment of various molecular events for nanotube and graphene based desalination are carried out by extensive molecular dynamics simulations. The understanding of driving forces associated to the filling of nanotubes with polar and non-polar fluids are explored. The coupling of transport coefficients with the thermodynamic entropy is provided in terms of universal scaling relation, which might be of great scientific and technological importance to the process endured with the phase transition like crystallization, nucleation and glass transition. The trend for water permeability and salt rejection with increasing pressure gradient, pore size and ion concentration are presented. The ultrafast fluidic nature for these membranes is captured from the breakdown of continuum model under nanoscale confinement which is reflected from the layered flow and plug like velocity profiles. The results revealed that the membranes comprising nanotubes of 1.0-1.1nm and graphene with width of  $h=7\text{\AA}$  show a great potential due to higher water permeability than TFC membrane.

**Keywords:** Seawater, Desalination, Diffusion, Permeation, Graphene nanomembrane, MD simulations.

### Introduction

Continuously increasing population, abnormal climate changes and rapid industrialization have intensified the problem of neat and clean potable water<sup>1</sup>. Even though nearly 71% of the earth crust is occupied by water, however, only 3% of this is fresh and suitable for human consumption. Many of the added impurities to these water sources by human beings and industries are non-biodegradable, and so are threatening not only to aquatic life but also if added to food-chain impose risk to human health<sup>2</sup>. One way to tackle this problem and increase the availability of drinking water is by treating the contaminated effluents to eradicate the impurities. Though the traditional methods such as ion exchange<sup>3</sup>, chemical precipitation<sup>4</sup>, solvent extraction and adsorption process<sup>5</sup> are widely used to remove the impurities from the contaminated water, however, their use at large scale is limited due to high operational cost, low permeate flux and inapplicability to handle effluents with low concentration of metal ions. Nowadays, the most widely adopted commercial desalination techniques are electro dialysis, nanofiltration<sup>6</sup> and reverse osmosis (RO)<sup>7</sup>. In RO method, water is forced through a semi-permeable membrane, that blocks the

passage of solutes and only water is allowed to pass through. However, a significant energy input is needed for this process to pressurize the feed water above osmotic pressure so that the useful flux can be obtained. Although ROs are believed to be of greatest practical potential, the water permeability is still not satisfactory. Also, the energy and capital consumption are quite intensive. However, since the energy cost of the RO process depends on the nature of solute to be filtered and the characteristics of membrane being used, the raised issue can be managed by selecting the appropriate membrane for the process<sup>8</sup>. At present, thin-film composites (TFCs) are the most common membranes being used in this process<sup>9</sup>. These are polysulfone or polyethersulfone membranes coated with polyamide layer, which provide them narrow, tortuous but continuous pores. These pores are suitable for flow of water but reject the salt ions. TFC membranes provide high salt rejection efficiency but suffer with the problem of low water permeability. After the implausible studies of Hummer *et al.*<sup>10</sup> for ultrafast water transport through CNT(6,6), a particular interest has been focused on nanotube based membranes<sup>11, 12</sup>. Due to large surface to volume ratio and excellent thermal, chemical and mechanical properties, nanotubes have attracted a broad interest for membrane applications<sup>13, 14</sup>. The experimental studies by Hind *et al.*<sup>15</sup> and Holt *et al.*<sup>16</sup> showed the extraordinary fast water transport through smaller diameter double walled CNT membranes, which was also revalidated by Joseph *et al.*<sup>17</sup> using MD simulations. However, later on, Thomas *et al.*<sup>18</sup> reported much smaller enhancement in water transport through these nanotubes compared to what was reported by Holt *et al.*<sup>16</sup>. Subsequently, the studies by Naguib *et al.*<sup>19</sup> as well as Major *et al.*<sup>20</sup> showed that the increment in flow decreases with increase in nanotube diameter. Also, Su *et al.*<sup>21</sup> reported the exponential relationship between water flux and nanotube length/diameter. To be noted, the filling of nanotubes is surprising as the nanotube like hydrophobic confinement are generally supposed to decrease both the entropy and enthalpy due to breakage of water-water hydrogen bond (HB) network while entering in the nanotube confinement. In spite of unfavourable energies, the water molecules not only spontaneously fill up the nanotube but also contribute to enhanced conduction rate, exceeding the hydrodynamic predictions of Hagen-Poiseuille<sup>10, 16</sup>. The filling and emptying transitions in hydrophobic channels have been explained by many authors using different analytical, quantum, and molecular dynamics calculations<sup>22-24</sup>. However, as far as thermodynamic criteria are concerned, there are contradictory views on whether the spontaneous filling of nanotubes is driven by the entropy or energy transfer. Vaitheeswaran *et al.*<sup>25</sup> reported the

zero entropy of transfer from bulk into a quasi-infinite nanotube channels using statistical mechanical framework. Pascal *et al.*<sup>23</sup> as well as Kumar *et al.*<sup>24</sup> explained that the water entry inside CNTs is favoured by entropy but unfavored by enthalpy. The translational entropy of water transfer inside CNT(6,6) was reported to increase by Pascal *et al.*<sup>23</sup>, but was shown to be reduced by Kumar *et al.*<sup>24</sup>. Such contradictions require additional studies in order to arrive at a reasonable conclusions. Since the increase in translational entropy of confined water is expected to arise from the tetrahedral liberation of bulk water and therefore might be expected to be unique to water, and so the question, whether enhancement in translational entropy is really unique to water remains open both from the experimental tests and simulation studies. In addition, only scarce studies are available on the structural and transport properties of other polar and nonpolar fluids for nanotube confinement, which need to be explored.

Considering the potential applicability of nanotube membranes, it is important to explore the mechanism involved in ultrafast fluid-transport, and frictionless flow through nanotubes. Also, a precise assessment of nanotubes is necessary before selecting them as a potential candidate for future desalination. However, since the fabrication methodologies of nanotubes are yet to be simplified, the computational studies become main source for directing this field. Also, high-fidelity molecular simulations provide a better understanding of the process from microscopic point of view<sup>26</sup>. In this regard, the molecular dynamics simulations<sup>27</sup> have been used to understand the associated mechanism of fluid transport through nanochannels membranes. Extensive MD simulations using LAMMPS<sup>26</sup> and GROMACS<sup>28</sup> package were conducted. The sp<sup>2</sup> carbon atoms of the CNTs has been modelled as Lennard-Jones particle with size and energy parameters as  $\sigma_{cc} = 3.4\text{\AA}$  and  $\epsilon_{cc} = 0.36\text{kJ/mol}$  respectively. The long range electrostatic interactions between atoms and molecules were determined using Ewald method<sup>29</sup> and the short range interactions are incorporated with L-J potential. For water SPC potential<sup>30</sup> and for other fluids OPLS force field parameters<sup>31</sup> are used. The thermodynamic parameters in this study have been estimated using very efficient and robust two phase thermodynamic (2PT) method<sup>32,33</sup>. The simulation systems were equilibrated for 50ns, followed by 20ns of production run. Further, the coordinates and velocities were saved after each 4fs for calculation of dynamical parameters and ~500fs for structural one. MD trajectories were visualized by VMD package<sup>34</sup>.

## Results and discussion

### Fluid transport through CNT(6,6)

The internal space wetting of hydrophobic CNT(6,6) with water (@300K) and methane (@136K) results from favourable free energies inside the CNT as shown in Table 1.

**Table 1** Entropy, energy, and free energy gain (in unit J/mol-K) for confined water and methane.

| CNT(6,6) | $\Delta S$ | $T\Delta S$ | $\Delta E$ | $\Delta A$ |
|----------|------------|-------------|------------|------------|
| Water    | 17.63      | 5.29        | 3.18       | -2.11      |
| Methane  | 22.23      | 2.84        | 2.75       | -0.09      |

The free energy of confined fluid is primarily favoured by increased translational and rotational entropies but largely by increased rotational entropy (Table 2). Our results explain that, yes, the nano confinement favours the translational entropy of transfer

**Table 2.** Entropy components (J/mol-K) and density (g/cm<sup>3</sup>) of water (H<sub>2</sub>O) and methane (CH<sub>4</sub>).

| System                  | $S_{\text{trans}}$ | $S_{\text{rot}}$ | $S_{\text{total}}$ | density |
|-------------------------|--------------------|------------------|--------------------|---------|
| bulk H <sub>2</sub> O   | 51.46              | 14.96            | 66.42              | 0.981   |
| bulk CH <sub>4</sub>    | 49.55              | 30.03            | 79.58              | 0.427   |
| H <sub>2</sub> O in CNT | 56.12              | 27.93            | 84.05              |         |
| CH <sub>4</sub> in CNT  | 51.55              | 48.48            | 100.43             |         |

from bulk solution to CNT and the gain in translation entropy is not unique to water like H bonding fluid but is also observed for nonpolar methane. As shown in Fig.1, the water molecules inside CNT were found in ordered structure but in zig-zag orientation to form the H bond with their neighbours. Interestingly, the methane molecules inside CNT were also found in ordered structure, irrespective of their inability to form H bond as shown in Fig.1. In fact, the single file arrangement of water and methane in CNT(6,6), leads to higher diffusion than conventional confinement. The results demonstrate that though H-bonding plays an important role in conduction, it is not the only driving factor, as the nonpolar fluids, which do not have any H bond can not only go inside CNT but also flow through it. The associated driving forces for filling and transport of fluid are due to enhanced translational and rotational entropies, which are credited by strong correlation among confined fluid molecules (increased translational entropy) and availability of more free space for rotation of molecules (enhanced rotational entropy)<sup>35</sup>.

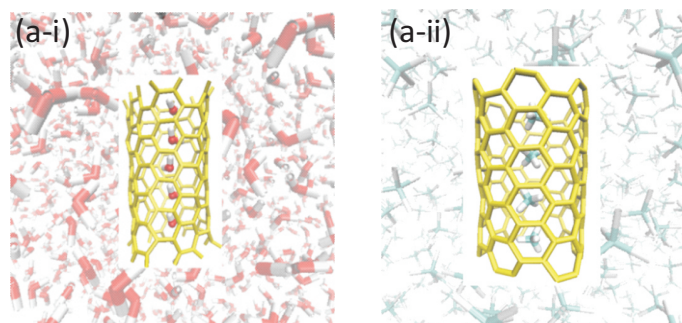


**Fig. 1:** Snapshot of (a-i) water and (a-ii) methane molecules inside CNT(6,6).

### Effect of CNT termination and polarization

Here, the effect of nanotube charge and CNT end termination was explored by studying the water structure, dynamics and thermodynamics through unterminated, terminated neutral and terminated-charged CNT(6,6) as shown in Fig.2(a). Hydrogenated pores were obtained by functionalizing edge carbon atoms of CNT with hydrogen atoms of size and energy parameter as  $\sigma_{\text{HH}} = 2.5\text{\AA}$ ,  $\epsilon_{\text{HH}} = 0.1255\text{kJ/mol}$ . The atomic charges for CNT atoms were determined by performing ab initio quantum<sup>36</sup> calculations at the B3LYP/TZ2P<sup>36</sup> level of theory using ADF package<sup>37</sup>. Fig.2(b) reveals that the magnitude of partial charges at nanotube ends is much greater than the middle region. The dissimilarities in entropic components as reported in Table 3 were found to be correlated with various dynamical and structural parameters.

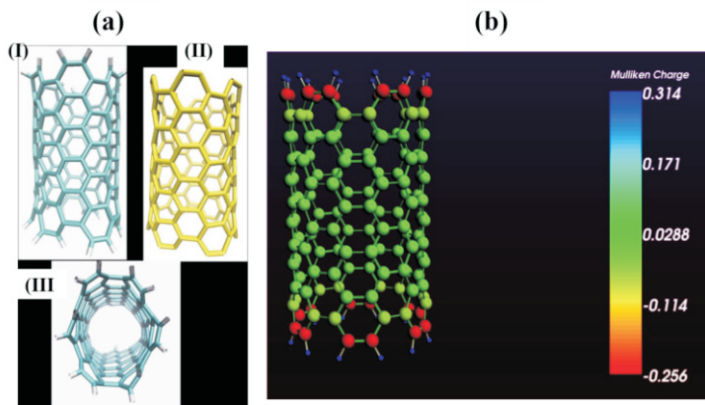


**Fig.2:** (a) Structure of CNTs: I and II. front view of H terminated and unterminated and III. top view of H terminated CNT (b) Partial charge distribution for H terminated CNT.

Fig.2(b) reveals that the magnitude of partial charges at nanotube ends is much greater than the middle region. The dissimilarities in entropic components as reported in Table 3 were found to be correlated with various dynamical and structural parameters. The rotational entropies are well corroborated with hydrogen bond (HB) correlation functions. Results revealed that the HBs of CNT confined water molecules show long preserving correlation if their rotations inside CNT are restricted by nanotube polarization. A relation between translational diffusivity and configurational entropy for water in bulk to CNTs is framed. The observed effects are too small to be realized in practical applications<sup>38</sup>.

**Table 3** Entropy components for bulk water and water confined in various CNTs.

| System                | $S_{trans}$          | $S_{rot}$            | $S_{total}$ |
|-----------------------|----------------------|----------------------|-------------|
| bulk H <sub>2</sub> O | 51.46 ( $\pm 0.25$ ) | 14.96 ( $\pm 0.06$ ) | 66.42       |
| un                    | 56.12 ( $\pm 0.20$ ) | 27.93 ( $\pm 0.01$ ) | 84.06       |
| tn                    | 56.97 ( $\pm 0.15$ ) | 31.45 ( $\pm 0.15$ ) | 88.42       |
| tc                    | 57.63 ( $\pm 0.17$ ) | 25.20 ( $\pm 0.19$ ) | 82.83       |

### Flow transition with nanotube diameter

The flow transition from sub-continuum to continuum regime was captured for water, methanol and methane with increasing nanotube diameter as displayed in Fig.3. The results show that the single file flow of fluid inside CNT is diminished with increase in tube diameter and renewed to layered flow for larger CNTs<sup>39</sup>. Such a transition was further described in terms of diffusion coefficient and density of states (DOS)<sup>39</sup>. The observations from DOS (Fig.4) was in good agreement with the corresponding velocity auto correlation function and diffusion dynamics<sup>40,41</sup>.

### Relation between diffusivity and entropy

Furthermore, we established a scaling relation for liquids in bulk and confined states. Since, it is very difficult to estimate the accurate diffusivity of fluids confined in CNT like one dimensional geometry from the experiments, linking them with the experimentally

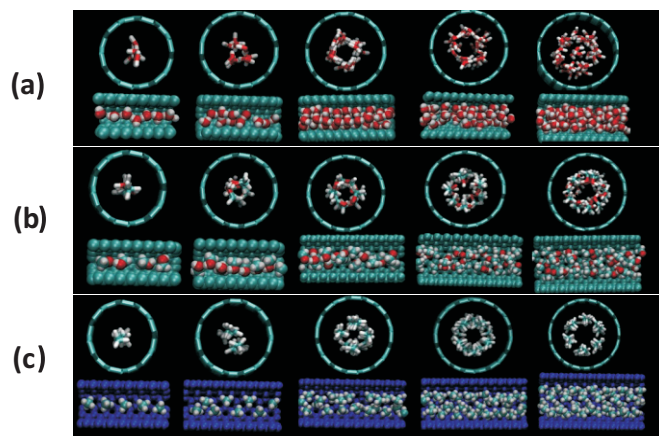


**Fig.3:** Snapshot of (a) water (b) methanol and (c) liquid methane inside CNT(6,6), CNT(7,7), CNT(8,8), CNT(9,9) and CNT(10,10) respectively.

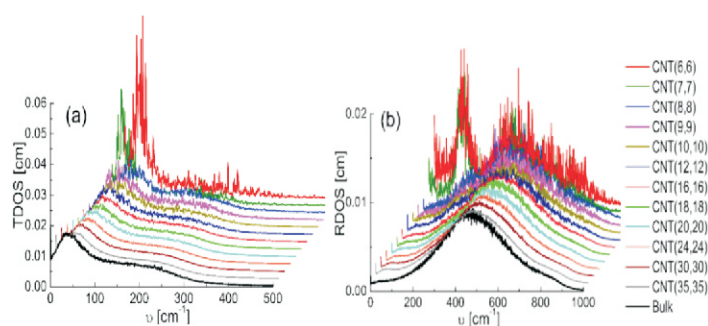


**Fig.4:** (a) Translational DOS (b) Rotational DOS for water in CNT confinement.

accessible thermodynamic quantities would be a great scientific and technological benefits.

Our results demonstrate persuasively that there exists a universal scaling relation between scaled diffusivity  $D^*$  and excess entropy  $S_{ex}$  for molecular fluids. However,  $D^*$  for molecular fluids ( $D_m^*$ ) differs from Dzugutov  $D^*$  by the scaling factor  $\alpha$ , which depends on structural correlation and the reduced density of molecular systems as shown by Eqns. 1 to 3.

$$D^* = A [\exp(B \cdot S_{ex})] \quad (1)$$

Where  $D^*$  is the scaled diffusivity,  $D^* = D\Gamma^{-1} \sigma^{-2}$  with  $\sigma$  is the hard sphere diameter and  $\Gamma$  as Enskog collision frequency,

$$\Gamma = 4\sigma^2 g(\sigma) \rho \left( \frac{\pi k_B T}{m} \right)^{1/2} \quad (2)$$

In this expression,  $m$  and  $\rho$  represent the molecular mass and density of the system respectively. The quantity  $\sigma$  is determined from position of first peak in pair correlation function and  $g(\sigma)$  is the value of pair correlation function at  $\sigma$ .  $D_m^*$  for molecular fluids ( $D_m^*$ ) differs from Dzugutov  $D^*$  by the scaling factor  $\alpha$

$$D_m^* = \alpha \cdot D_{Dzugutov}^* \quad (3)$$

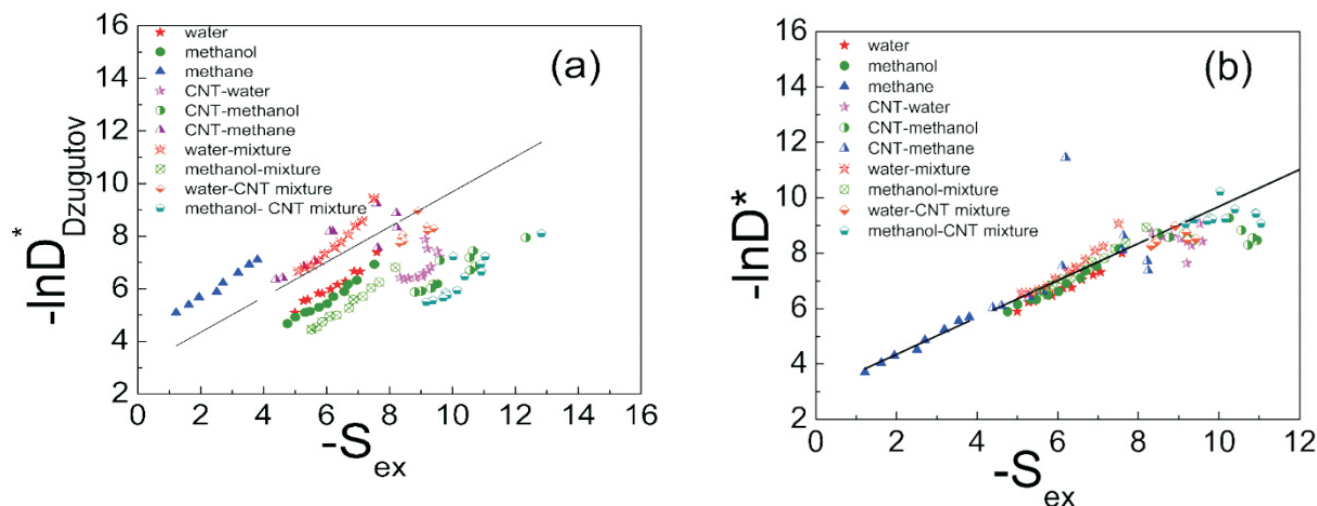


**Fig.5:** Scaling relation for  $D^*$  and  $S_{ex}$  with (a) Dzugutov equation (b) Modified relation of  $Dm^*$  and  $S_{ex}$ .

Where  $\alpha = \left( \lambda \cdot C \left( \frac{g(\sigma)}{\rho^* \sigma} \right) \right)$ ,  $\lambda$  and  $C$  are constants:

(i) If  $\eta < 0.45$ ;  $\lambda = 0.4$  and  $C = 1$  for pure,  $C = 1/2$  for mixture and  $C = 1/7$  for CNT confinement.

(ii) If  $\eta > 0.45$ ;  $\lambda = 7.2$  and  $C = 1$  for pure,  $C = 1/10$  for mixture and  $C = 2/7$  for CNT confinement.  $\eta$  is the packing fraction, given by

$$\eta = \frac{\pi}{6} \rho^*$$

Interestingly, the simulation results of liquid argon indicate that  $\alpha$  reduces to one for atomic fluids. In other words, the proposed scaling equation represents Dzugutov relation in the limiting conditions where strong intra-molecular interactions can be waved off. The proposed scaling relation (Fig.5) covers the diverse set of hydrogen bonding fluids both in bulk and mixed state. Moreover, it has been shown that the validity of the proposed relation is not limited to the domain of conventional fluids but also can be reasonably used for CNT confinement. The results demonstrate that the connection between self-diffusivity and excess entropy is nearly universal for varieties of molecular liquids, liquid mixtures and liquids under nano-confinement if the structural effects caused by strong intramolecular and intermolecular interactions are taken care by  $g(\sigma)$  i.e. confinement by first shell of neighbour atoms and reduced density  $\rho^*$  in the scaling factor  $\alpha$ .<sup>42</sup> Applicability of the relation for CNT confinement manifest the transferability of proposed scaling equation from cage diffusion to molecular hopping like special diffusion mechanism<sup>42</sup>.

### Nanosopic assessment filtration in CNT

Subsequently, the nanoscopic view of desalination through CNT membranes using MD simulations has been explored. The

graphene terminated CNTs were used to represent the part of nanotube membrane as shown in Fig.6.

The trend for water permeability and salt rejection with increasing pressure gradient, nanotube diameter and salt concentration was evaluated and results are shown in Fig.7. Results reveal that the membranes comprising nanotubes of 1.0–1.1 nm diameter can be used for efficient water desalination with more than 95% salt rejection. The average permeability of water was estimated to be  $10^{-3}$  moles/cm<sup>2</sup>-sec-MPa, two order higher than TFC membranes.

Further, the water flux anomalies in CNT were found to be linked with the hydration characteristics of ions inside CNTs. It was noticed that akin to bulk phases, the mass transport through CNT can be linked with the diffusivity of component species<sup>43</sup>. It was seen that not only the diffusivities of water and ions, but also the

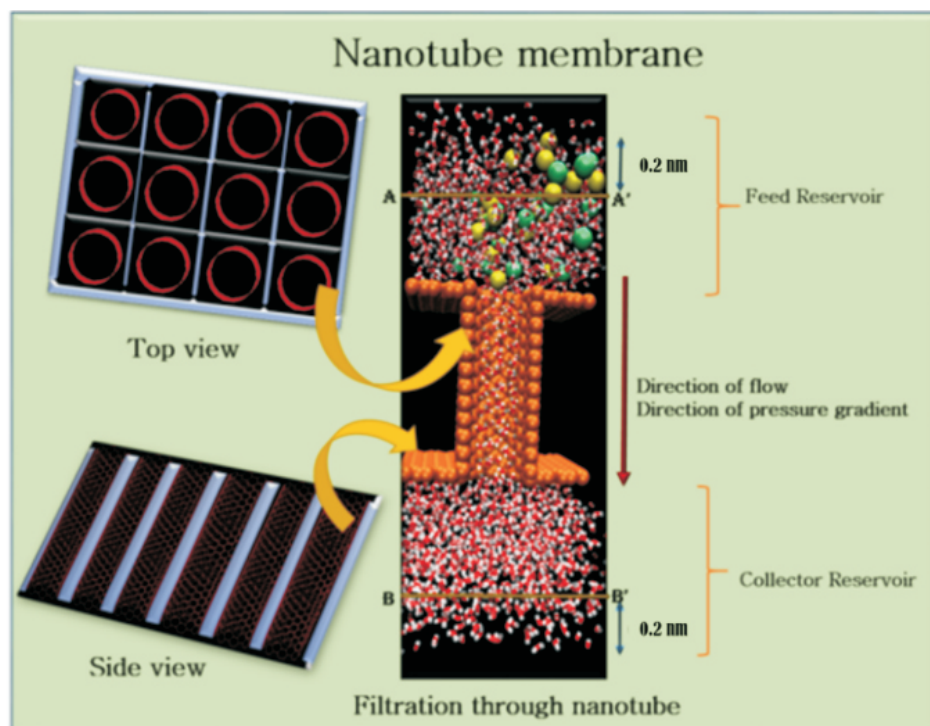


**Fig.6:** Schematic diagram of CNT membrane (green:  $Cl^-$ , yellow:  $Na^+$ , red and white represents O and H atoms of water, CNT shown by orange).

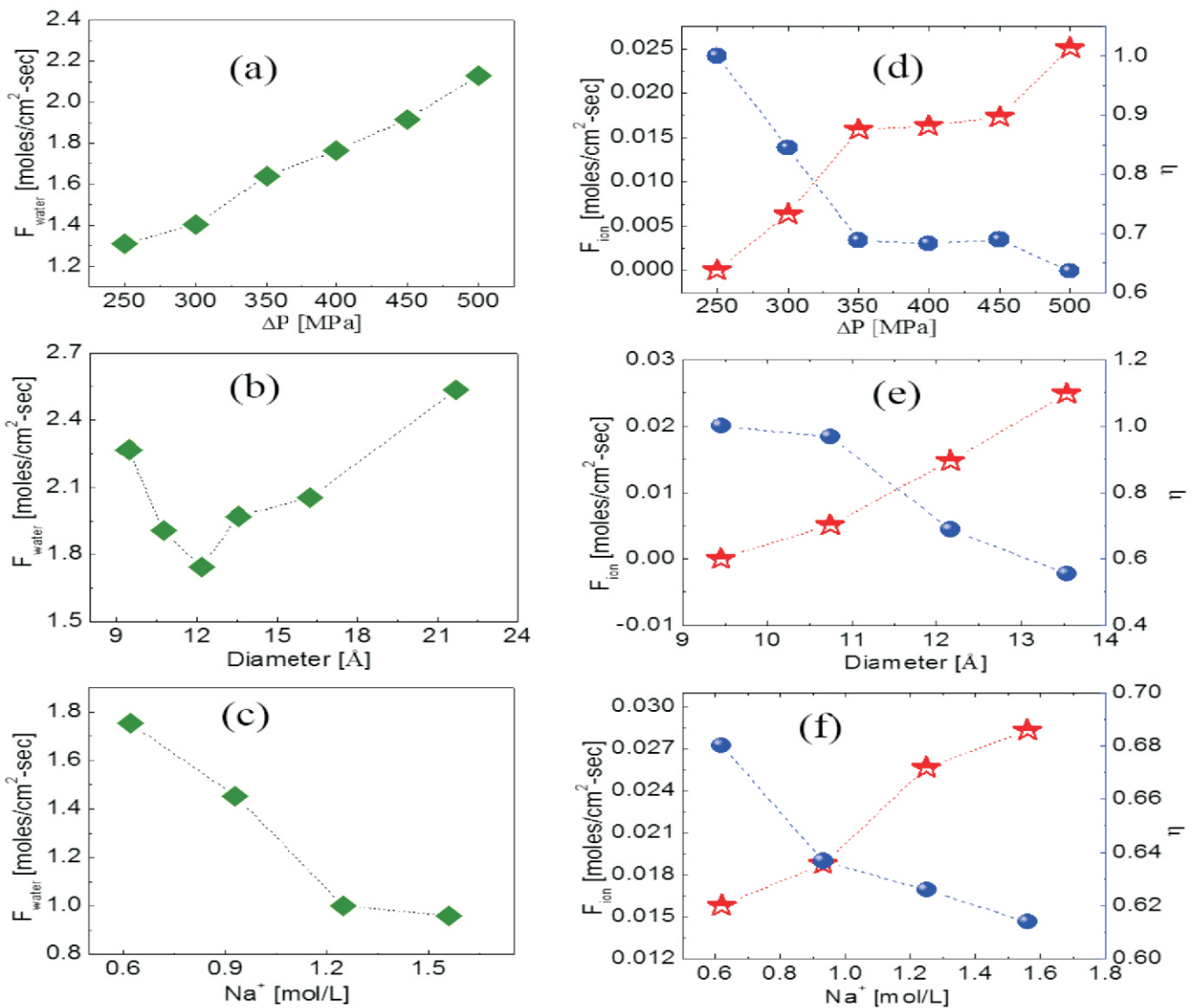


**Fig.7:** (a, b, c) flux of water  $F_{\text{water}}$  and (d, e, f) flux of ions  $F_{\text{ion}}$  (unit moles/cm<sup>2</sup>-sec) (left Y-axis) and salt rejection efficiency  $\eta$  (right Y-axis) as an effect of (a, d) pressure gradient (b,e) nanotube diameter and (c, f) feed concentration.

ratio of diffusivity  $D_{\text{water}}/D_{\text{ion}}$  can be linked with the respective water to ion flux ratio and the salt rejection trends<sup>43</sup>.

### Nanoscopic filtration in graphene

Further, in quest of identifying an inexpensive and easily scalable material with graphene like fluidic properties, the fluid transport through graphene membranes was investigated. The graphene membranes were made by tailoring of graphene sheets as shown in Fig.8. Results showed increasing water flux with increase in pore size, on the other hand, reducing water flux with increase in salt concentration. It was observed that no ion could pass through the membrane for  $h = 7\text{\AA}$ , indicating 100% salt rejection with pores of  $5\text{\AA}$ - $7\text{\AA}$ . However, it was reduced to 91.67% for  $h = 8\text{\AA}$  and 33.33% for  $h = 9\text{\AA}$  (Fig.9). The water permeability through the graphene channel ( $h = 7\text{\AA}$ ) is two orders of magnitude higher than TFC membrane. The breaking of continuum assumption in graphene nanopores was captured by the appearance of a layered water structure and plug-like velocity profiles<sup>44</sup>.

The fluidity under nano confinement of graphene was examined in terms of shear viscosity, friction coefficient and slip length. The calculated viscosity and diffusion coefficient under the graphene pores did not follow the Stokes–Einstein relation, indicating the failure of the hydrodynamic theory. The confined state of water in the graphene pores was also explored via the translational density of states and entropy, which displayed a significant change in the

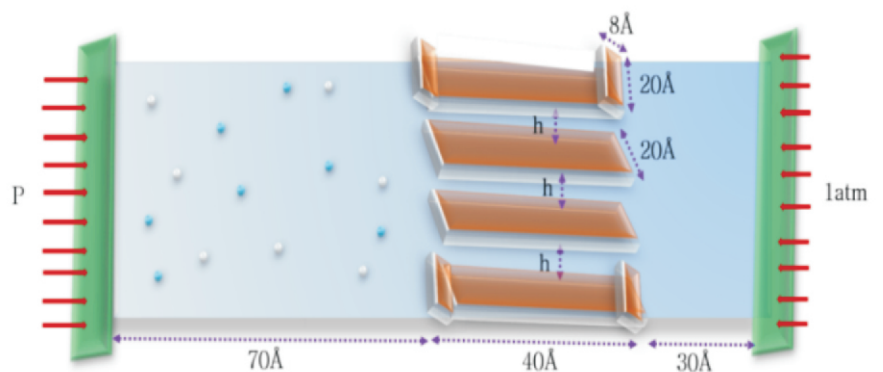


**Fig.8:** Schematic graphene membrane.

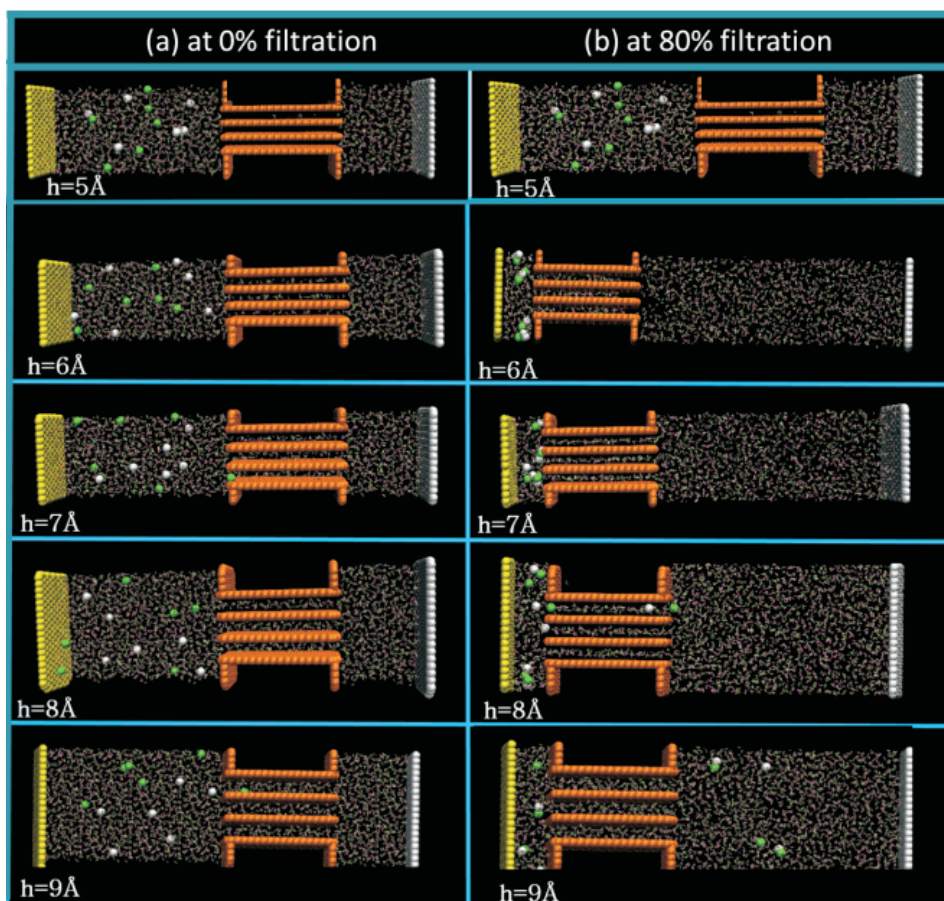


**Fig.9:** Snapshot for water filtration through graphene membrane with different width  $h = 5\text{--}9\text{\AA}$  taken at (a)  $t=0\text{ns}$  and (b) when 80% water has filtered from feed reservoir [ $C=0.2\text{M}$ ,  $P=150\text{Mpa}$ ].

translational entropy with change in the pore size and applied pressure and thus revealed the interconnectivity of the structure<sup>44</sup>.

## Conclusions

The results show that the wetting of the internal space of nanotubes with polar and nonpolar fluids results from the favourable free energy of confinement. The free energy of confined fluid is primarily favoured by increased entropy. The MD results suggest that the uneven membrane is beneficial. The proposed new scaling relations can be applied successfully for all the liquids and liquid mixtures in bulk and CNT confinement to capture the quantitative relationship of self-diffusion coefficient and excess entropy. The work concludes that the membranes comprising nanotubes of 1.0–1.1 nm diameter and graphene membranes of width  $h=7\text{\AA}$  show a great potential to be used in RO, as water permeability is much higher than TFC membrane. Overall, the understanding of fluid transport through nanotubes by MD simulations was fruitfully achieved. Linking of mass flux with diffusion and linking of diffusion with the experimentally accessible thermodynamic parameter entropy can be of great importance in various fields of science and technology. Also, the presented microscopic understandings might be helpful in examining the performance of other nano-membranes as well as biological channels.

## Acknowledgement

Computer division is acknowledged for providing Anupam super computation facility. We are grateful to K.T. Shenoy, Group Director, Chemical Engineering Group and S. Mukhopadhyay, Head, Chemical Engineering Division for encouragement.

## Corresponding Author\*

Sk. Musharaf Ali (musharaf@barc.gov.in)

## References

- [1] United Nations World Water Assessment Programme, The world water development report, Paris, France: UNESCO, 2014.
- [2] T. Masciangioli and W.X. Zhang, *Environ. Sci. Technol.*, 2003, 102A–108A.
- [3] A. Da browski, D.Z. Hubicki, P. Podkościelny and E. Robens, *Chemosphere*, 2004, **56**, 91-106.
- [4] M.T. Alvarez, C. Crespo and B. Mattiasson, *Chemosphere*, 2007, **66**, 1677-1683.
- [5] P.A. Brown, S.A. Gill and S.J. Allen, *Water Res* 34, 2000, **16**, 3907–3916.
- [6] M. Whitby, L. Cagnon, M. Thanou and N. Quirke, *Nano Lett.*, 2008, **8**, 2632-2637.
- [7] S.T. Oyama and S.M. Stagg-Williams, Inorganic, polymeric and composite membranes, Elsevier, Amsterdam, The Netherlands, 2011.
- [8] K. Takeuchi, Y. Takizawa, H. Kitazawa, M. Fujii, K. Hosaka, J. Ortiz-Medina, A. Morelos-Gómez, R. Cruz-Silva, M. Fujishige, N. Akuzawa and M. Endo, *Desalination*, 2018, **443**, 165-171.

- [9] M. Thomas and B. Corry, *Phil. Trans. R. Soc. A*, 2016, **374**, 20150020-20150020.
- [10] G. Hummer, J.C. Rasaiah and J.P. Noworyta, *Nature*, 2001, **414**, 188-190.
- [11] Z.E. Hughes, C.J. Shearer, J. Shapter and J.D. Gale, *J. Phys. Chem. C*, 2012, **116**, 24943-24953.
- [12] M. Majumder, N. Chopra and B. J. Hinds, *ACS Nano*, 2011, **5**, 3867-3877.
- [13] W. Zhang, P. Sherrell, A.I. Minett, J.M. Razal and J. Chen, *Energy Environ. Sci.*, 2010, **3**, 1286-1293.
- [14] J. Sengupta, in *Handbook of Nanomaterials for Industrial Applications: Micro and Nano Technologies*, 2018, pp. 172-194.
- [15] B.J. Hinds, N. Chopra, T. Rantell, R. Andrews, V. Gavalas and L. G. Bachas, *Science*, 2004, **303**, 62-65.
- [16] J.K. Holt, H.G. Park, Y. Wang, M. Stadermann, A.B. Artyukhin, C.P. Grigoropoulos, A. Noy and O. Bakajin, *Science*, 2006, **312**, 1034-1037.
- [17] P. Joseph, C. Cottin-Bizonne, J.-M. Benoit, C. Ybert, C. Journet, P. Tabeling and L. Bocque, *Phys. Rev. Lett.*, 2006, **97**, 156104-156104.
- [18] J.A. Thomas and A.J.H. McGaughey, *Nano Lett.*, 2008, **8**, 2788-2793.
- [19] N. Naguib, H. Ye, Y. Gogotsi, A.G. Yazicioglu, C.M. Megaridis and M. Yoshimura, *Nano Lett.*, 2004, **4**, 2237-2243.
- [20] R.C. Major, J.E. Houston, M.J. McGrath, J.I. Siepmann and X.Y. Zhu, *Phys. Rev. Lett.*, 2006, **96**, 177803-177804.
- [21] J. Su and H. Guo, *J. Phys. Chem. B*, 2012, **116**, 5925-5932.
- [22] A. Waghe, J.C. Rasaiah and G. Hummer, *J. Chem. Phys.*, 2002, **117**, 10789-10795.
- [23] T.A. Pascal, W.A. Goddard and Y. Jung, *Proc. Natl. Acad. Sci. U.S.A.*, 2011, **108**, 11794-11798.
- [24] H. Kumar, B. Mukherjee, S.T. Lin, C. Dasgupta, A.K. Sood and P.K. Maiti, *J. Chem. Phys.*, 2011, **134**, 124105-124108.
- [25] S. Vaitheeswaran, J.C. Rasaiah and G. Hummer, *J. Chem. Phys.*, 2004, **121**, 7955-7965.
- [26] S. Plimpton, *J. Comput. Phys.*, 1995, **117**, 1-19.
- [27] D. Frenkel and B. Smit, *Understanding molecular simulation: from algorithms to applications*, Academic press., Elsevier, United States, 2001.
- [28] S. Pronk, R. Schulz, P. Larsson, P. r. Bjelkmar, R. Apostolov, M.R. Shirts, J.C. Smith, P.M. Kasson, D. v. d. Spoel, B. Hess and E. Lindahl, *Bioinformatics*, 2013, **29**, 845-854.
- [29] T. Darden, D. York and L. Pedersen, *J. Chem. Phys.*, 1993, **98**, 10089-10092.
- [30] H.J.C. Berendsen, J.R. Grigera and T.P. Straatsma, *J. Phys. Chem.*, 1987, **91**, 6269-6271.
- [31] W.D. Cornell, P. Cieplak, C.I. Bayly, I.R. Gould, K.M. Merz, J. Ferguson, D.M.,D.C. Spellmeyer, T. Fox, J. W. Caldwell and P.A.A. Kollman, *J. Am. Chem. Soc.*, 1995, **117**, 5179-5197.
- [32] S.-T. Lin, M. Blanco and W.A. Goddard, *J. Chem. Phys.*, 2003, **119**, 11792-11805.
- [33] S.-T. Lin, P.K. Maiti and W.A. Goddard, *J. Phys. Chem. B*, 2010, **114**, 8191-8198.
- [34] W. Humphrey, A. Dalke and K. Schulten, *J. Mol. Graphics*, 1996, **14**, 33-38.
- [35] P. Sahu, S.M. Ali and K.T. Shenoy, *J. Chem. Phys.*, 2015, **142**, 074501-074511.
- [36] G.Y. Guo and J.C. Lin, *Phys. Rev. B*, 2005, **71**, 165402-165412.
- [37] G.t. Velde, F.M. Bickelhaupt, E.J. Baerends, C.F. Guerra, S. J.A.v. Gisbergen, J.G. Snijders and T. Ziegler, *J. Comput. Chem.*, 2001, **22**, 931-967.
- [38] P. Sahu and S.M. Ali, *J. Chem. Phys.*, 2015, **143**, 184503-184514.
- [39] P. Sahu, S.M. Ali and K.T. Shenoy, *AIP Conf. Proc.*, 2016, **1731**, 110050-110053.
- [40] P. Sahu and S. M. Ali, *J. Chem. Eng. Data*, 2017, **62**, 2307-2315.
- [41] P. Sahu and S.M. Ali, *Int J Quantum Chem.*, 2017, e25578.
- [42] P. Sahu, S.M. Ali and K.T. Shenoy, *J. Phys. Chem. C*, 2017, **121**, 11968- 11974.
- [43] P. Sahu, S.M. Ali, K.T. Shenoy and S. Mohan, *Phys. Chem. Chem. Phys.*, 2019, **21**, 8529-8542.
- [44] P. Sahu, S.M. Ali, K.T. Shenoy and S. Mohan, *Phys. Chem. Chem. Phys.*, 2019, **21**, 21389-21406.